Luminescent Self-Assembled Monolayer on Gold Nanoparticles: Tuning of Emission According to the Surface Curvature

Angela Candreva [1,2], Giuseppe Di Maio [1], Francesco Parisi [1], Francesca Scarpelli [1], Alessandra Crispini [1], Nicolas Godbert [1], Loredana Ricciardi [2], Antonello Nucera [3], Carmen Rizzuto [3], Riccardo C. Barberi [2,3], Marco Castriota [2,3] and Massimo La Deda [1,2,*]

[1] Department of Chemistry and Chemical Technologies, University of Calabria, 87036 Rende, Italy; angela.candreva@unical.it (A.C.); giuseppe.dimaio@unical.it (G.D.M.); francesco.parisi@unical.it (F.P.); francesca.scarpelli@unical.it (F.S.); a.crispini@unical.it (A.C.); nicolas.godbert@unical.it (N.G.)
[2] Institute of Nanotechnology (NANOTEC), National Research Council (CNR), UOS Cosenza, 87036 Rende, Italy; loredana.ricciardi@cnr.it (L.R.); riccardo.barberi@fis.unical.it (R.C.B.); marco.castriota@fis.unical.it (M.C.)
[3] Department of Physics, University of Calabria, 87036 Rende, Italy; antonello.nucera@unical.it (A.N.); carmen.rizzuto@unical.it (C.R.)
* Correspondence: massimo.ladeda@unical.it

Instrumental set-up and photophysical methods

Spectrofluorimetric grade solvents were used for the photophysical investigations in solution, at room temperature. Solid samples are prepared by placing microcrystalline powder between two quartz windows, and spectra have been recorded in an instrumental front-face geometry.

A Perkin Elmer Lambda 900 spectrophotometer was employed to obtain the absorption spectra.

Steady-state emission spectra were recorded on a HORIBA Jobin-Yvon Fluorolog-3 FL3-211 spectrometer equipped with a 450 W xenon arc lamp, double-grating excitation and single-grating emission monochromators (2.1 nm/mm dispersion; 1200 grooves/mm), and a Hamamatsu R928 photomultiplier tube. Emission spectra are confirmed by excitation ones. Emission and excitation spectra were corrected for source intensity (lamp and grating) and emission spectral response (detector and grating) by standard correction curves [9-11].

Time-resolved measurements were performed using the time-correlated single-photon counting (TCSPC) option on the Fluorolog 3. NanoLED at 265 nm, fwhm <1.0 ns with repetition rate at 1 MHz, was used to excite the sample. Excitation sources were mounted directly on the sample chamber at 90° to a single-grating emission monochromator (2.1 nm/mm dispersion; 1200 grooves/mm) and collected with a TBX-04-D single-photon-counting detector. The photons collected at the detector are correlated to the excitation pulse by a time-to-amplitude converter (TAC). Signals were collected using an IBH Data Station Hub photon-counting module, and data analysis was performed using the commercially available DAS6 software (HORIBA Jobin Yvon IBH). Goodness of fit was assessed by minimizing the reduced Chi squared function ($\chi 2$) and visual inspection of the weighted residuals.

Emission quantum yields were determined using the optically dilute method on aerated solutions which absorbance at excitation wavelengths was < 0.1; 2-aminopyridine in ethanol was used as standard ($\Phi = 0.37$) [12].

The experimental uncertainty on the molar extinction coefficients is 1%, while on the emission quantum yields is 5%. The examined compounds are fairly stable in solution, as demonstrated by the constancy of their absorption spectra over a week.

Micro-Raman spectra [13-16] were collected using a Horiba-Jobin Yvon [17] microprobe apparatus with spectral resolution ~2 cm^{-1}, equipped with a CCD (256 x 1024 pixels) detector cooled at −70°C. The spectra were collected by using two laser sources: a 532 nm line of a diode laser, with an emitted power of 50 mW and a 633 nm line of He-Ne laser

with an emitted power of 17 mW power, equipped with edge/notch filters. The solutions have been characterized by using the 4× and 20× Mplan Olympus objectives while the films have been characterized by using the 50x Mplan Olympus objective, focusing a laser spot of about 1 μm of apparent diameter. To avoid structural changes due to laser heating, a 0.3-OD filter has been used to collect Raman spectra: the actual intensity of the transmitted radiation is 50% of the intensity of the laser emitted radiation.

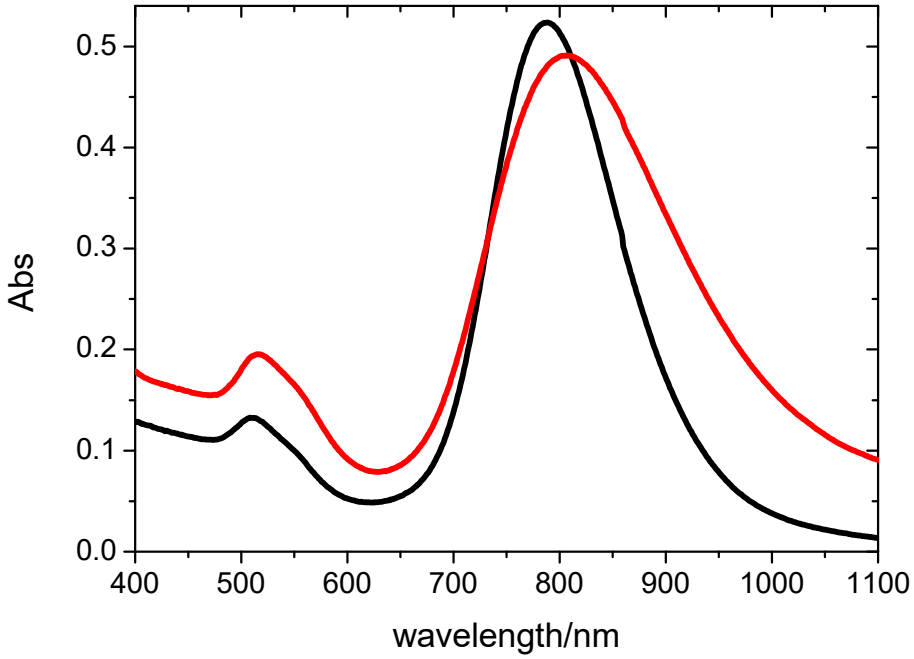

Figure S1. Extinction spectrum of $AuNR_{CTAB}$ in water (black line) and of $AuNR_{PEG\text{-}SH}$ in dichloromethane (red line).

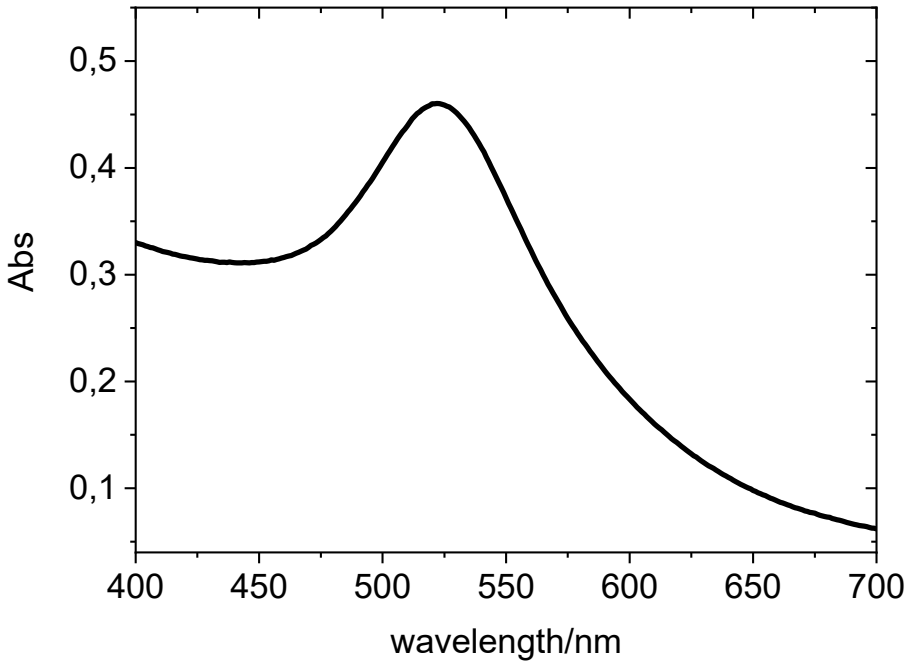

Figure S2. Extinction spectrum of $AuNS_{SC}$ in water.

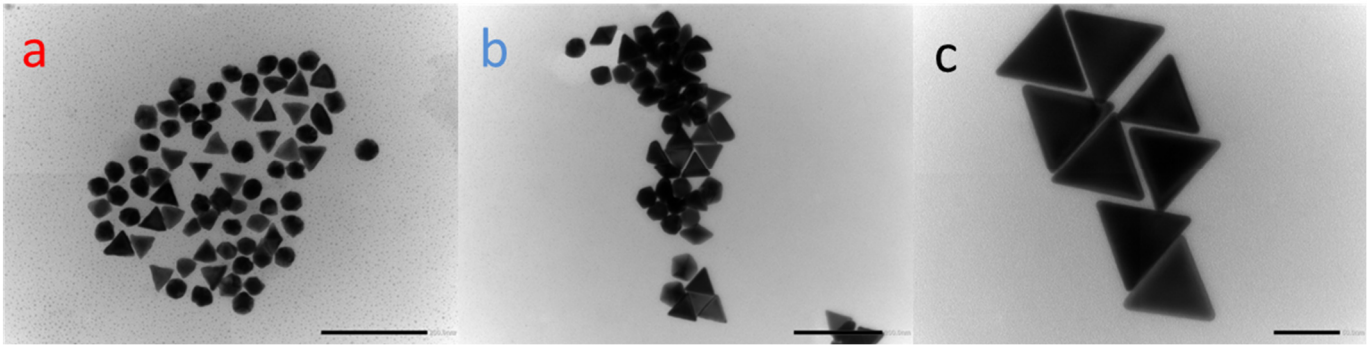

Figure S3. TEM images of the obtained nanoparticles (see § 2.3 in the main text) before the selective precipitation (a); after precipitation: supernatant (b) and precipitate (c)

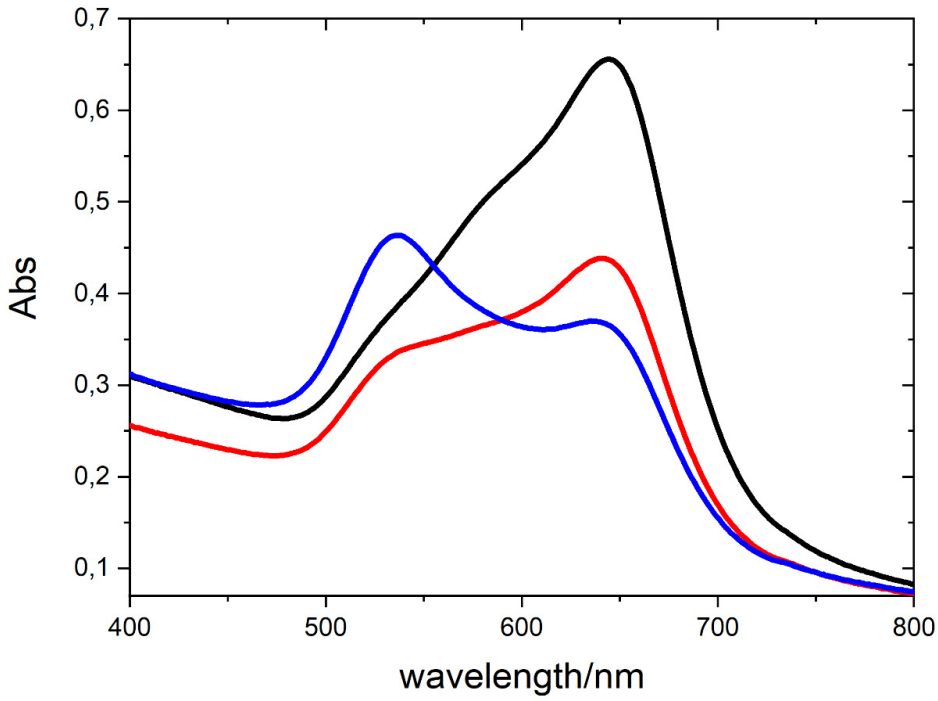

Figure S4. Extinction spectra of nanoparticles solutions before the selective precipitation (red line); after precipitation: supernatant (blue line) and precipitate (black line) containing $AuNT_{CTAC}$ purified nanoparticles (see Figure S3 for the correspondent TEM image).

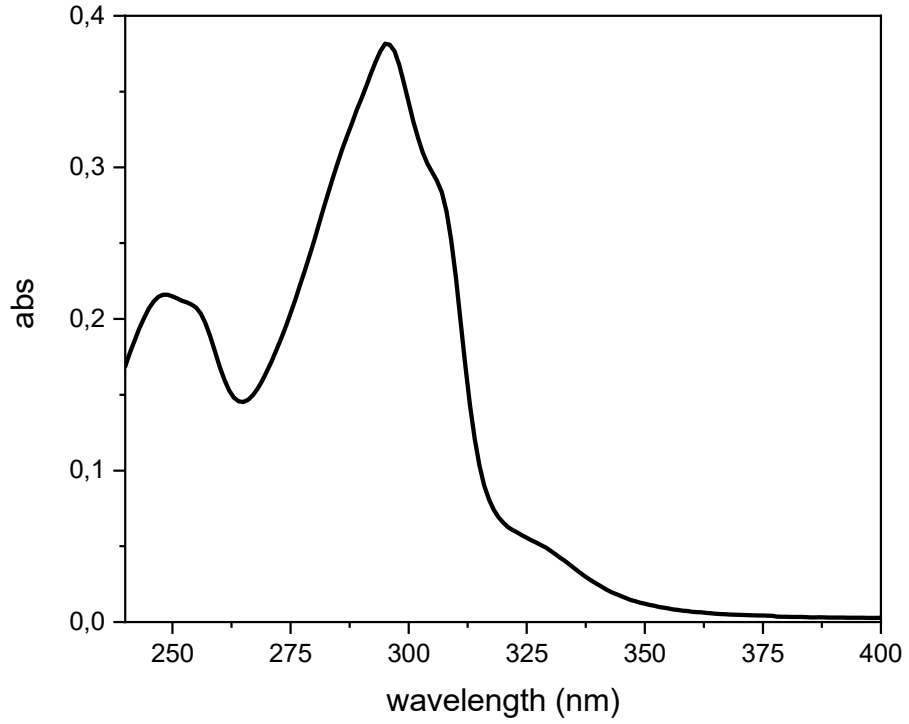

Figure S5. Absorption spectrum of Bpy-SH in diluted dichloromethane solution (1.3 E-5 M).

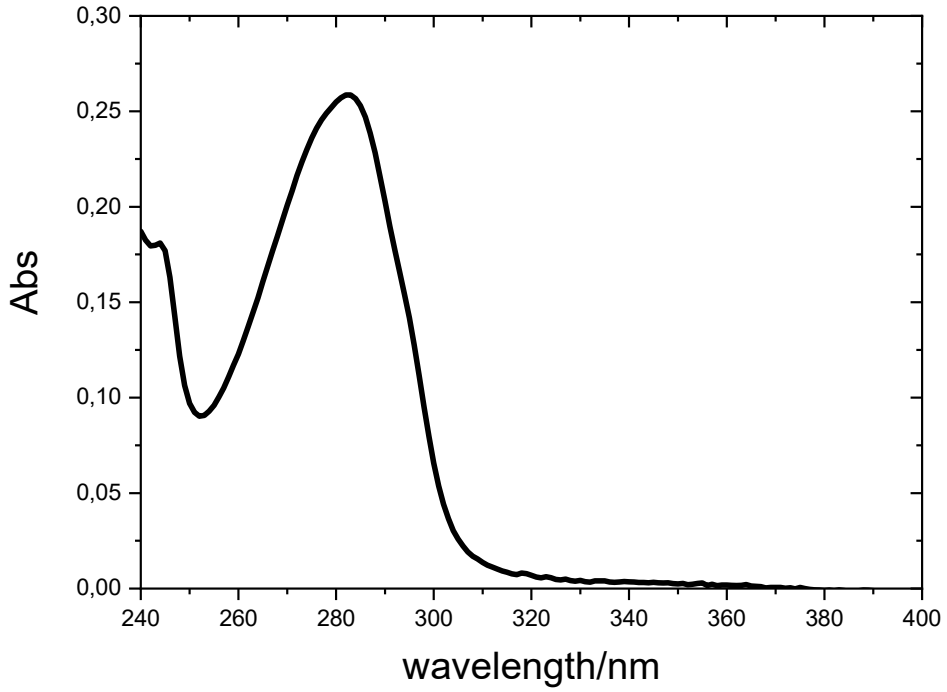

Figure S6. Absorption spectrum of 2,2'-bipyridine in diluted dichloromethane solution (1.3 E-5 M).

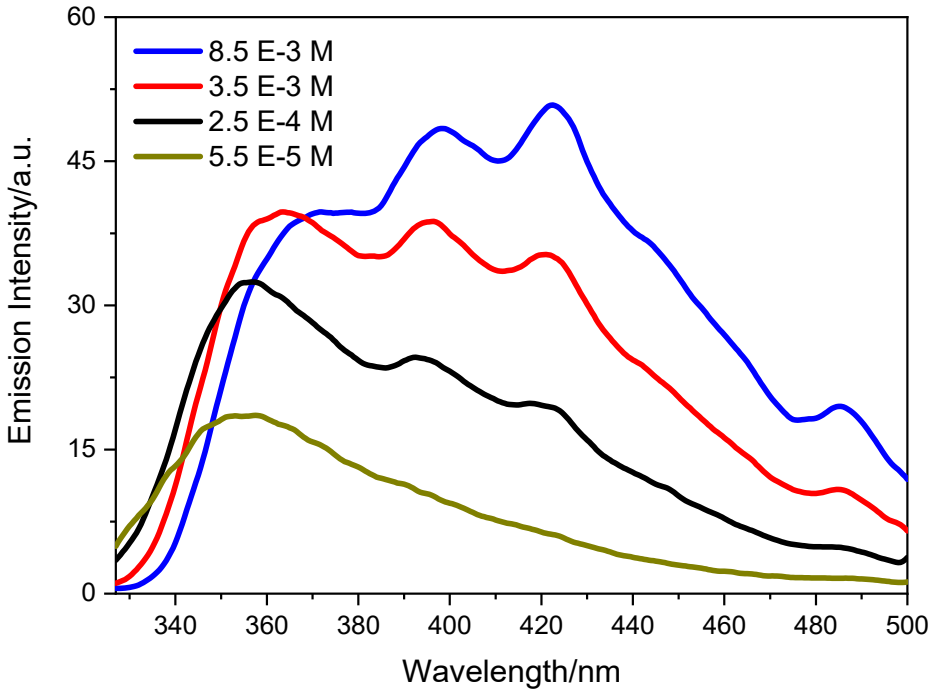

Figure S7. Emission spectra of Bpy-SH dichloromethane solutions at various concentrations (λ_{ex} = 306 nm)

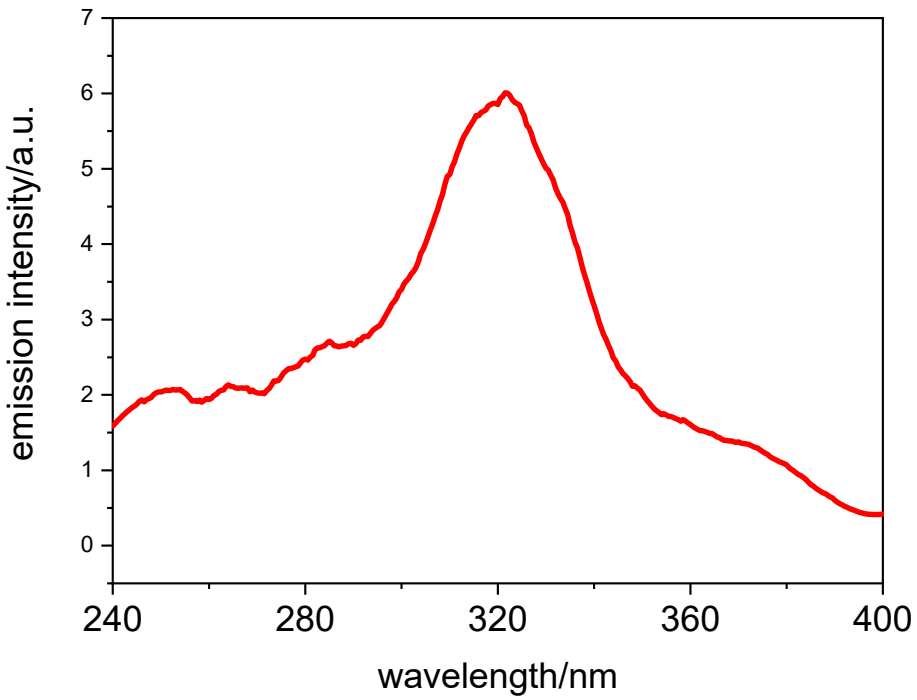

Figure S8. Excitation spectrum of **Bpy-SH@AuNR** in water solution (λ_{em} = 350 nm)

The attribution of the Raman modes has been quite difficult, because in literature it has been not possible to find the theoretical Raman spectra of the Bpy-SH with the nitrogen atoms in configuration trans. Anyway, a tentative attribution of the Raman bands shown in the spectra of Figure 2 has been done by comparison with others comparable systems and it has been reported in Table S1.

Table S1. Raman modes attribution of Bpy-SH in powder sample.

Raman mode (cm^{-1})	Assignment [1]	Assignment [2]	Assignment [3]	Assignment [4]
392		Sym Au - ν_7 ring o.p def (out of plane modes)		
431	τ(CCCC)16b' (Out of plane Vibration)	Sym Ag – ν_{14} interring i.p. bend (In plane modes)		
462	β(C'C)15' (In plane Vibration)			
569	π(CC_α)10a (Out of plane Vibration)	Sym Bu - ν_6 ring o.p. def+interring o.p. bend+CH o.p. bend (out of plane modes)		
631	β(CCC)6b' (In plane Vibration)	Sym Ag - ν_{13} ring i.p. def (In plane modes) + Sym Bu - ν_{13} ring i.p. def (In plane modes)		
660		Sym Bu - ν_{15} ring i.p. def (out of plane modes)	Ring i.p. def.	Ring i.p. def.
713			Ring breath	Ring breath
777	τ(CCCC)4' (Out of plane Vibration)	Sym Ag - ν_{12} ring i.p. def. (In plane modes) + Sym Au – ν5 ring o.p. def+interring o.p. bend+CH o.p. bend (out of plane modes)		
793		Sym Au - ν_4 CH o.p. bend (out of plane modes)		
843	β(CCC)12' (In plane Vibration)	Sym Bg - ν_4 interring o.p. bend+CH o.p. bend (out of plane modes)	CH o.p. bend	CH o.p. bend
1020		Sym Bu - ν_{12} ring i.p. def + ring str (In plane modes)		
1120	β(CH)18a' (In plane Vibration)	Sym Bu - ν_8 CH i.p. bend (In plane modes)	CH i.p. def. + ring str	CH i.p. def. + ring str.
1216				CH2 Wagging
1241	ν(C-C)19a (In plane Vibration)	Sym Ag - ν_7 ring str (In plane modes)	Inter-ring stretch + ring str. + CH i.p. def	Inter-ring stretch + ring str. + CH i.p. def
1261		Sym Bu – ν_5 + ν_7 ring str + CH i.p. bend (In plane modes)		
1304		Sym Ag - ν_6 interring str+ring str+ring i.p. def (In plane modes)		
1323		Sym Ag - ν_5 CH i.p. bend + interring i.p. bend (In plane modes)	Inter-ring str. + ring str. + CH i.p. def.	Inter-ring str. + ring str. + CH i.p. def.
1407		Sym Bu - ν_4 CH i.p. bend + ring str (In plane modes)	CH2 Wagging	CH2 Wagging
1498	ν(C-C)19a (In plane Vibration)	Sym Ag – ν_3 CH i.p. bendCring str (In plane modes)	CH i.p. def. + ring str	CH i.p. def. + ring str.
1596	ν(C-N)8b (In plane Vibration)	Sym Ag - ν_1 ring str (In plane modes)	Ring str.	Ring str.
2566	ν(S-H) [5]			
2937	ν(CH_2 asym) [5]			
i.p., in-plane; o.p., out-of-plane; def, deformation; str, stretching.				

The spectra collected on PEG-SH powder is shown in Figure S9 in order to be used as reference for the Raman study performed on the others samples.

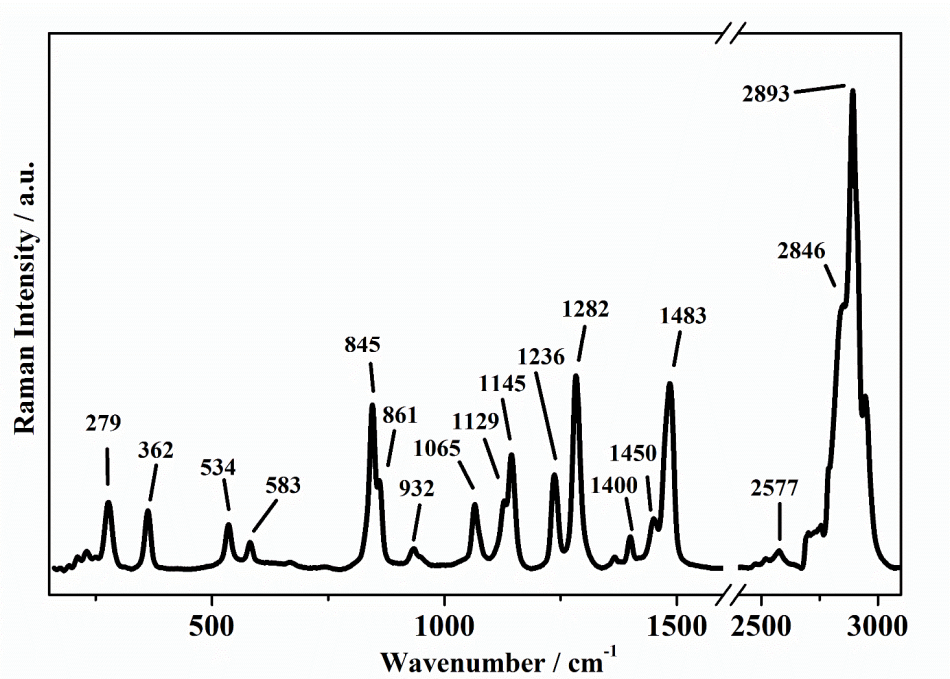

Figure S9. Raman spectrum of PEG-SH in powder sample collected in the ranges between 150 and 1600 cm^{-1} and between 2400 and 3100 cm^{-1} (laser source at 532 nm)

In table S2 is reported the assignment of each Raman band of the spectra of figure S9 collected on the PEG-SH powder. Such assignment has been done by comparison with similar substance since it was not possible to find a theoretical spectrum of the Polyethylene glycol 2-mercaptoethyl methyl ether (PEG-SH). Nevertheless, the attribution fit very well with the experimental spectrum.

Table S2. PEG-SH Raman modes and their attribution.

Raman mode (cm^{-1})	Assignment [6]
279	Sym A_1; δ $(COC)_i$, δ (COC)
362	Sym E_1; δ $(COC)_0$, δ $(OCC)_i$
534	Sym E_1; δ $(OCC)_0$,
583	Amorphous aggregation state
845	Sym E_1; r $(CH_2)_0$,
861	Sym A_1; r $(CH_2)_i$, ν $(CO)_i$
932	Amorphous aggregation state
1065	Sym E_1; r $(CH_2)_i$, ν $(CO)_i$
1129	Sym A_1; ν (CC), ω (CH_2)
1145	Sym A_1; ν $(CO)_0$,
1236	Sym E_1; t $(CH_2)_i$, t $(CH_2)_0$
1282	Sym E_1; t $(CH_2)_i$, t $(CH_2)_0$
1400	Sym A_1; ω $(CH_2)_i$, ν (CC),
1450	Sym E_1; δ $(CH_2)_i$,
1483	Sym A_1; δ $(CH_2)_i$,
2577	ν (S-H stretching) [5,7]
2846	ν (CH_2 stretching) [5,7,8]
2893	ν (CH_2 stretching) [5,7,8]

Raman spectra have been collected also on gold nanorods functionalized by PEG-SH dispersed in water ($AuNR_{PEG-SH}$). In figure S10 it is shown the Raman spectra collected on $AuNR_{PEG-SH}$ by the laser source at 532nm in the ranges between 200 and 1800 cm^{-1} and between 2500 and 3800 cm^{-1}.

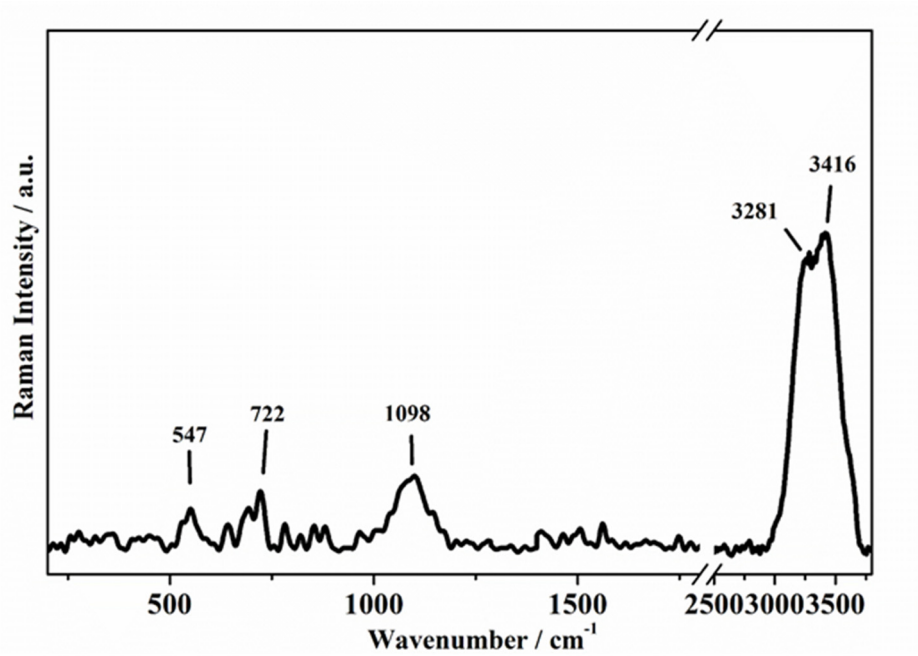

Figure S10. Raman spectrum of PEG-SH in powder sample collected in the ranges between 150 and 1600 cm^{-1} and between 2400 and 3100 cm^{-1} (laser source at 532 nm)

As it is possible to see in figure S10, there are many small Raman bands that fall below 1200 cm^{-1} which can be assigned to the PEG-SH. The typical Raman bands of the cetyltrimethylammonium bromide (CTAB) [18] at 763 cm^{-1}, 962 cm^{-1} and 2847 cm^{-1} are not detectable. It means that the CTAB has been completely removed during the synthesis of the $AuNR_{PEG\text{-}SH}$ samples [19-22]. The others two bands at 3281 $cm^{-1}$and 3416 cm^{-1} (Figure S10) are assigned to the O-H stretching of the solvent H_2O [23].

References

1. Kühnle, A. Self-Assembly of Organic Molecules at Metal Surfaces. *Curr. Opin. Colloid Interface Sci.* **2009**, *14*, 157–168.
2. Chaki, N.K.; Vijayamohanan, K. Self-Assembled Monolayers as a Tunable Platform for Biosensor Applications. *Biosens. Bioelect ron.* **2002**, *17*, 1–12.
3. Motealleh, A.; Dorri, P.; Kehr, N.S. Self-Assembled Monolayers of Chiral Periodic Mesoporous Organosilica as a Stimuli Responsive Local Drug Delivery System. *J. Mater. Chem. B* **2019**, *7*, 2362–2371.
4. Gankin, A.; Mervinetsky, E.; Alshanski, I.; Buchwald, J.; Dianat, A.; Gutierrez, R.; Cuniberti, G.; Sfez, R.; Yitzchaik, S. ITO Work Function Tunability by Polarizable Chromophore Monolayers. *Langmuir* **2019**, *35*, 2997–3004.
5. Love, J.C.; Estroff, L.A.; Kriebel, J.K.; Nuzzo, R.G.; Whitesides, G.M. Self-Assembled Monolayers of Thiolates on Metals as a Form of Nanotechnology. *Chem. Rev.* **2005**, *105*, 1103–1170.
6. Laibinis, P.E.; Whitesides, G.M.; Allara, D.L.; Tao, Y.T.; Parikh, A.N.; Nuzzo, R.G. Comparison of the Structures and Wetting Properties of Self-Assembled Monolayers of n-Alkanethiols on the Coinage Metal Surfaces, Copper, Silver, and Gold. *J. Am. Chem. Soc.* **1991**, *113*, 7152–7167.
7. Heister, K.; Allara, D.L.; Bahnck, K.; Frey, S.; Zharnikov, M.; Grunze, M. Deviations from 1:1 Compositions in Self-Assembled Monolayers Formed from Adsorption of Asymmetric Dialkyl Disulfides on Gold. *Langmuir* **1999**, *15*, 5440–5443.
8. Hamoudi, H.; Esaulov, V.A. Selfassembly of α,ω-Dithiols on Surfaces and Metal Dithiol Heterostructures. *Ann. Phys.* **2016**, *528*, 242–263.
9. F. Scarpelli, A. Ionescu, L. Ricciardi, P. Plastina, I. Aiello, M. La Deda, A. Crispini, M. Ghedini, N. Godbert, A novel route towards water-soluble luminescent iridium(III) complexes via a hydroxy-bridged dinuclear precursor, Dalton Trans., 2016, 45, 17264-17273

10. P. F. Liguori, M. Ghedini, M. La Deda, N. Godbert, F. Parisi, R. Guzzi, A. Ionescu, I. Aiello, Electrochromic behaviour of Ir(III) bis-cyclometalated 1,2-dioxolene tetra-halo complexes: fully reversible catecholate/semiquinone redox switches. Dalton Transactions 2020, 49, 2628–2635.
11. A. Ionescu, R. Caligiuri, N. Godbert, A. Candreva, M. La Deda, E. Furia, M. Ghedini, I. Aiello, New electropolymerizable Ir(III) complexes with -ketoiminate ancillary ligands. Chemistry - An Asian Journal 2019, 14, 3025–3034.
12. T. Mutai, J. D. Cheon, G. Tsuchiya, K. Araki, Tuning of fluorescence properties of aminoterpyridine fluorophores by N-substitution. Journal of the Chemical Society. Perkin Transactions 2 2002, 2, 862–865.
13. O. Poizat, G. Buntinx, P. Valat, V. Wintgens, M. Bridoux, Photochemistry of 4,4'-Bipyridine. Nanosecond Absorption and Raman Study of the Hydrogen Atom Abstraction from Methanol and 2-Propanol Journal of Physical Chemistry 1993, 97, 5905–5910.
14. J. Kumar, R. Thomas, R. S. Swathi, K. G. Thomas, Au nanorod quartets and Raman signal enhancement: towards the design of plasmonic platforms Nanoscale 2014, 6, 10454–10459.
15. X. Gao, Reproducibility in Surface-Enhanced Raman Spectroscopy.Journal of Physical Chemistry 1990, 94, 6858–6864.
16. T. Yang, H. Long, M. Malkoch, E. K. Gamstedt, L. Berglund, A. Hult, Characterization of Well-Defined Poly(ethylene glycol) Hydrogels Prepared by Thiol-ene Chemistry Polimer Chemistry,2011, 4044–4054.
17. L. Ducasse, M. Dussauze, J. Grondin, J. C. Lassègues, C. Naudin, L. Servant, Spectroscopic study of poly(ethylene oxide)6 : LiX complexes (X=PF6 , AsF6 , SbF6 , ClO4) Physical Chemistry Chemical Physics, 2003, 5, 567–574.
18. M. Kertesz, C. H. Choi, S. Y. Hong, Conformational Information from Vibrational Spectra of Polyaniline. Synthetic Metals 1997, 85, 1073–1076.
19. Z. Zhang and M. Lin, Fast loading of PEG–SH on CTAB-protected gold nanorods, RSC Adv., 2014, 4, 17760- 17767.
20. Serrano-Montes AB, De Aberasturi DJ, Langer J, et al (2015) A General Method for Solvent Exchange of Plasmonic Nanoparticles and Self-Assembly into SERS-Active Monolayers. Langmuir 31:9205–9213. https://doi.org/10.1021/acs.langmuir.5b01838
21. Yüce M, Kurt H (2017) How to make nanobiosensors: Surface modification and characterisation of nanomaterials for biosensing applications. RSC Adv 7:49386–49403. https://doi.org/10.1039/c7ra10479k
22. Conde J, Dias JT, Grazú V, et al (2014) Revisiting 30 years of biofunctionalization and surface chemistry of inorganic nanoparticles for nanomedicine. Front Chem 2:1–27. https://doi.org/10.3389/fchem.2014.00048
23. A. V. Whitney, R. P. Van Duyne and F. Casadio, An innovative surface-enhanced Raman spectroscopy (SERS) method for the identification of six historical red lakes and dyestuffs, J. Raman Spectrosc., 2006, 37, 993–1002.